Thermal Expansion and Phase Formation of ZrW_2O_8 Aerogels

L. D. Noailles,[†] H.-h. Peng,[‡] J. Starkovich,[‡] and B. Dunn*,[†]

Department of Materials Science and Engineering, UCLA, Los Angeles, California 90095-1595, and Northrop Grumman Space Technology, Redondo Beach, California 90278

Received August 25, 2003. Revised Manuscript Received January 22, 2004

Aerogels with the nominal composition ZrW_2O_8 have been prepared by pore solvent exchange with liquid CO_2 followed by supercritical drying. These aerogels are amorphous and can be tailored to have extremely high surface areas. Thermal expansion is measured for the amorphous aerogel as well as the aerogel post thermal treatment. The cubic phase forms at 900 °C in less than 30 s. The cubic phase prepared this way has a large negative thermal expansion coefficient of -10.5×10^{-6} °C^{-1} as shown by variable temperature X-ray diffraction.

Introduction

ZrW_2O_8 exhibits large isotropic negative thermal expansion over its entire stability range ($\alpha = -9.07 \times 10^{-6}$ K^{-1} from 0.3 to 350 K).[1] This property lends itself to applications requiring dimensional thermal stability, which includes a wide variety of areas from electronics and optics, to sensors and actuators, to dental-filling materials. For most of these applications, it is envisioned that cubic ZrW_2O_8 is used as filler in a composite material. A recent analysis highlighted the correlation between the particle size of the filler material and the thermal expansion of the composite.[2,3] For smaller filler particles, especially for nanoscale particles, there is a decrease in thermal expansion of the composite due to an increase in the interfacial region between the filler and matrix materials. Also, as demonstrated by gold nanoparticles, nanoscale materials may exhibit surprisingly unique thermal expansion properties when compared to their bulk counterparts.[4] Nanoparticles of cubic ZrW_2O_8 have not been reported due to difficulties in processing. Attempts to mechanically decrease the particle size of as-synthesized cubic ZrW_2O_8 results in amorphization, and amorphization has been reported even by grinding in an agate mortar.[5]

Although cubic ZrW_2O_8 is thermodynamically stable over a narrow temperature range (1105−1257 °C),[6] once formed it is kinetically stable up to ∼770 °C. The cubic phase is formed in the solid-state reaction between ZrO_2 and $2WO_3$, but possibly due to volatilization of WO_3, the reaction does not reach completion even after several days at high temperatures (1230 °C) with intermittent grinding.[7] If the WO_3 volatilization is controlled by wrapping the sample in Pt foil and the sample is quenched, single-phase ZrW_2O_8 can be prepared by standard solid-state synthesis methods.

Several soft chemistry routes to cubic ZrW_2O_8 have been reported. Mixing aqueous solutions of zirconium oxynitrate and ammonium metatungstate yields a white precipitate that forms the desired single-phase product when heated to 1150 °C.[8] Refluxing the precipitate in HCl produces $ZrW_2O_7(OH)_2(H_2O)_2$, which can be dehydrated to form fairly pure cubic ZrW_2O_8 around 600 °C.[9] Cubic ZrW_2O_8 prepared at low temperatures from the hydrate was reported to have an average particle size close to 1 μm. A second preparatory route involves heating a mixture of WCl_3 suspended in $CHCl_3$ with a solution of zirconium isopropoxide 2-propanol complex dissolved in THF to 110 °C for a week in a sealed tube.[10] This results in an amorphous precipitate that transforms to cubic ZrW_2O_8 when heated to 1200 °C for 15 min. However, neither of these synthetic routes is suitable for the preparation of high surface area fillers for composite materials with dimensional thermal stability.

Aerogels are inherently nanomaterials, as they are a combination of empty pores and a framework matrix whose diameters and walls are on the order of nanometers.[11,12] Aerogels have high surface areas; thus, a ZrW_2O_8 aerogel composite will have a high interfacial region. The pores in an aerogel are interconnected in

* To whom correspondence should be addressed.
[†] UCLA.
[‡] Northrop Grumman Space Technology.

(1) Evans, J. S. O.; David, W. I. F.; Sleight, A. W. *Acta Crystallogr., Sect. B: Struct. Sci.* **1999**, *55*, 333−340.
(2) Ji, X. L.; Jing, J. K.; Jiang, W.; Jiang, B. Z. *Polym. Eng. Sci.* **2002**, *42*, 983−993.
(3) Park, C.-S.; Kim, M.-h.; Lee, C. *J. Mater. Sci.* **2001**, *36*, 3579−3587.
(4) Li, W. H.; Wu, S. Y.; Yang, C. C.; Lai, S. K.; Lee, K. C. *Phys. Rev. Lett.* **2002**, *89*, 135504.
(5) Perottoni, C. A.; daJornada, J. A. H. *Science* **1998**, *280*, 886−889.
(6) Chang, L. L. Y.; Scroger, M. G.; Philips, B. *J. Am. Ceram. Soc.* **1967**, *50*, 211−215.
(7) Evans, J. S. O.; Mary, T. A.; Vogt, T.; Sleight, A. W. *Science* **1996**, *272*, 90−92.
(8) Kameswari, U.; Slight, A. W.; Evans, J. S. O. *Int. J. Inorg. Mater.* **2000**, *2*, 333−337.
(9) Closmann, C.; Sleight, A. W.; Haygarth, J. C. *J. Solid State Chem.* **1998**, *139*, 424−426.
(10) Lind, C.; Wilkinson, A. P. *J. Sol−Gel Sci. Technol.* **2002**, *25*, 51−56.
(11) Rolison, D. R.; Dunn, B. *J. Mater. Chem.* **2001**, *11*, 963−980.
(12) Husing, N.; Schubert, U. *Angew. Chem. Int. Ed.* **1998**, *37*, 23−45.

10.1021/cm034791q CCC: $27.50
Published on Web 03/09/2004

three dimensions and should be large enough for penetration of the matrix material.

Here, we report the preparation of both network and precipitate gels with the nominal composition ZrW_2O_8 and aerogels prepared from these gels. The characterization carried out on these materials includes phase formation as a function of temperature, Raman, TEM, dilatometric measurements, and variable temperature X-ray diffraction. We have found that by using this sol−gel route, phase-pure cubic ZrW_2O_8 is formed in a very short time (<1 min) at temperatures within the thermodynamic stability range (1100−1250 °C). Starting from the aerogel, sub-micrometer cubic particles are made at the lower temperature of 900 °C with a reaction time of only 30 s. We also report the preparation of thin film ZrW_2O_8 using this chemistry.

Experimental Section

The ZrW_2O_8 sols were prepared by dissolving stoichiometric quantities of the zirconium isopropoxide 2-propanol complex ($Zr[OCH(CH_3)_2]_4 \cdot (CH_3)_2CHOH$, Aldrich 99.9%) and tungsten oxychloride ($WOCl_4$, Aldrich 98%) in anhydrous 2-propanol under an inert atmosphere. These reactions can also be carried out in ambient conditions without adverse effects. The ratio of Zr:2W precursor to the volume of 2-propanol was adjusted for the desired molarities of 0.5, 0.35, 0.25, 0.08, and 0.05 M. The reaction is exothermic and produces corrosive (HCl) vapors. Heating the mixture with stirring to 70−80 °C for 1 h resulted in a transparent sol. The reactants completely dissolve within minutes, and heating overnight results in no visible change. A 0.25 M sol prepared this way is stable for over 1 month at 25 °C if kept in a closed environment (to prevent hydrolysis). On exposure to the atmosphere, the sol hydrolyzes. The sol was allowed to gel at room temperature with stirring in an open container. The gelation time depends on the molarity and exposure conditions, but ranged between 1 h and 2 days. For molarities of 0.25 M or greater, the resulting gel is transparent, while for 0.08 M or less, a loosely connected white precipitate gel is formed. The 0.05 M sol did not form a rigid gel and could not be processed by the supercritical dryer. Allowing some of the solvent to evaporate by stirring the gel in an open container produced a sufficiently firm gel with the approximate molarity of 0.13 M. The container was sealed shortly after gelation and the gel was allowed to age for at least 2 days. The solvent in the pores of the gel was exchanged with liquid CO_2 for 1 week and dried supercritically.

The aerogels were subjected to a variety of heat treatments. Small samples were heated in platinum crucibles for 0.5, 2.5, and 30 min in 50 °C intervals. If warranted, heat treatments extended up to 3 days. The samples were placed directly in a preheated furnace and air-quenched after the designated time. The samples for Raman, TEM, and dilatometric measurements were prepared from the 0.13 M gel. One gram of the as-made 0.13 M aerogel was heated from 200 to 600 °C over 15 min (designated as sample 0.13M2). A total of 1 g (in 0.05-g portions) of the aerogel was placed directly into an oven preheated to 900 °C for 30 s (0.13M3). A 2-g sample of the aerogel was heated twice at 900 °C for 30 s and then at 1100 °C for 1.5 min (0.13M4).

The surface area and pore size of the aerogel were obtained from BJH analysis of adsorption and desorption isotherms using a Micromeritics ASAP 2010. X-ray diffraction data were collected using Cu Kα radiation with a diffractometer fitted with a graphite monochromator. Structural refinements were preformed using the GSAS suite of programs. Raman spectra were recorded on a Coherent Innova 90C-5 Argon Ion Laser with 514.5-nm excitation line and 100-mW power, 4-s integration, and a SPEX 1401 0.85-m Czerny-Turner double monochromator equipped with a C31034 PMT (cooled). Raman spectra were typically measured from 60 to 1100 cm^{-1}. A TA Instruments Thermomechanical Analyzer was used to obtain the dilatometer data. Data were collected from −150 to 155 °C with a heating and cooling rate of 5 °C min^{-1}. The coefficient of thermal expansion was calculated using the formula

$$\alpha = (l_{T2} - l_{T1})/[l_{T1}(T2 - T1)] \quad (1)$$

where l_{T1} is the length at temperature 1 and T1 is the temperature at temperature 1. A Perkin-Elmer Pyris Diamond TG/DTA was used to obtain the TGA/DTA data. For a typical TG/DTA measurement, samples were heated and cooled at 10 °C min^{-1} from room temperature to 1180 °C. A background correction was not applied to the TG or DTA data. Variable temperature X-ray diffraction data were collected on a Phillips PW 3040 diffractometer equipped with an Anton Paar HTK 1200 high-temperature oven and a X'celerator RTMS scanning detector.

Thin films were prepared by depositing the 0.5 M sol onto silicon wafers via dip or spin coating. The wafer was then placed directly in a preheated oven at 1150−1200 °C for 30 s to 1 h and quenched to room temperature in air. For multiple layer films, this sequence was repeated and the next layer was deposited after calcination of the previous one.

Results

Aerogels were prepared from sols of varying molarity and characterized after thermal treatments. Visually, the gels could be separated into network and precipitate gels, which are represented by the 0.35 and 0.13 M gels, respectively. The aerogels prepared from these two different types of gels are compared in terms of surface area, porosity, and thermal analysis. More detailed characterization including Raman spectroscopy, phase formation, and thermal expansion measurements is then presented for various thermal treatments of the 0.13 M gel because thermal treatments of the 0.35 M gel resulted in similar products with lower surface areas.

Porosity and Surface Area. The supercritically dried aerogels show an increase in pore size and surface area with decreasing molarity. The 0.35 and 0.13 M gels result in aerogels with average pore diameters of 6 and 11 nm and surface areas of 150 and 510 $m^2\ g^{-1}$ respectively. It should be noted that ZrW_2O_8 has a high formula weight (587 g mol^{-1}) and that a surface area of 510 $m^2\ g^{-1}$ for ZrW_2O_8 is equivalent to a much higher surface area (∼5000 $m^2\ g^{-1}$) for SiO_2. The higher molarity network gels have a much narrower pore size distribution than the lower molarity precipitate gels. The fwhm of the peak in the pore volume versus pore diameter curve increases from 5 to 57 nm for the 0.35 and 0.13 M aerogels, respectively.

Thermal Analysis. The TG curve (Figure 1a) of the 0.35 M aerogel indicates two regions of mass loss, one equivalent to 129 g/mol of ZrW_2O_8 from RT to 245 °C and the other equivalent to 43 g/mol of ZrW_2O_8 from 340 to 610 °C (Table 1). Although the first mass loss is mostly desorption and may contain both water and organics, the second may be due to the loss of a $CH(CH_3)_2$ group more strongly attached to the framework. The DTA curve (Figure 1b) reveals an endothermic peak that correlates to the first mass loss and two endothermic peaks and one exothermic peak (475 °C) over the temperature range of the second mass loss. There are two exothermic peaks (635 and 800 °C) and an endothermic peak at 1120 °C with a minimum at 1129 °C in the temperature region above the mass loss. It should be noted that the 635 and 800 °C exotherms

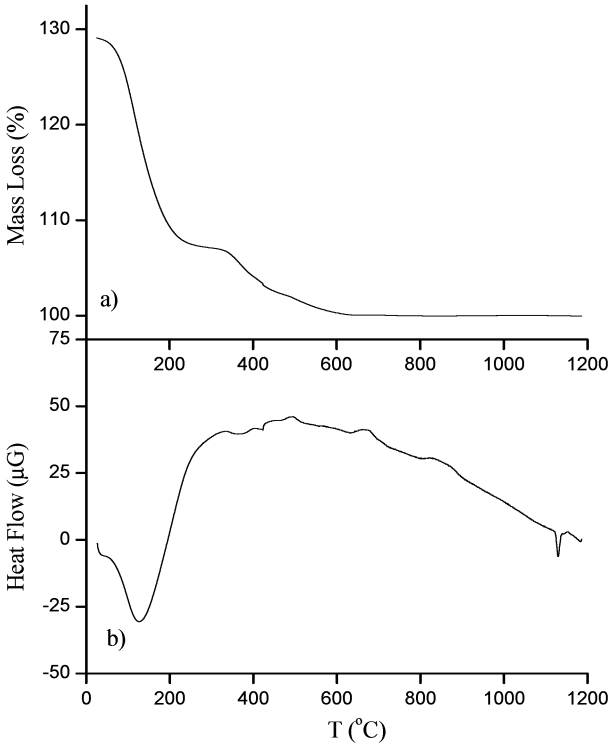

Figure 1. (a) TG data and (b) DTA data for the 0.35 M ZrW_2O_8 aerogel. Note that the lack of background subtraction in the DTA data results in a bell-shaped baseline.

Table 1. Summary of TG Data for the 0.35 M ZrW_2O_8 Aerogel

beginning temp (°C)	end temp (°C)	Δ mass (% normalized to ZrW_2O_8)	equivalent mass (g/mol)
50	245	22	129
340	610	7	43

are broad and end at 715 and 900 °C, respectively. As discussed below, these two exothermic peaks indicate crystalline phase formation of the trigonal (∼700 °C) and cubic phases (∼900 °C). The product of the TGA/DTA run was no longer a powder, but a hard pellet, indicating sintering and densification.

The TG curve of the 0.13 M aerogel (Figure 2) is distinctly different from the 0.35 M aerogel TG curve. This difference is due to the difference in the chemical makeup of the 0.13 M gel when compared to the 0.35 M gel. It indicates the lack of, or very soft, chemical bonding to the mixed metal oxide framework, and there is no higher temperature mass loss of 43 g/ZrW_2O_8 as there was for the 0.35 M gel. The one and only mass loss for the 0.13 M aerogel is smooth, starts at room temperature, and is completed by 450 °C. The DTA curve has two weak exothermic peaks, one around 650 °C and the other near 850 °C. These are followed by an endothermic peak at 1120 °C with a minimum at 1127 °C. Like the other aerogel, the product of the TGA/DTA measurement was a dense pellet. The low intensity of the DTA peaks may be due in part to the inherent lack of thermal conductivity because of the aerogel morphology and the small amount of sample that will fit into the sample pan because of the ultralow density.

Phase Formation. Equivalent thermal treatments of the various aerogels resulted in similar products. Thus, the details presented here for the 0.13 M aerogel can be extended to the other aerogel compositions. The

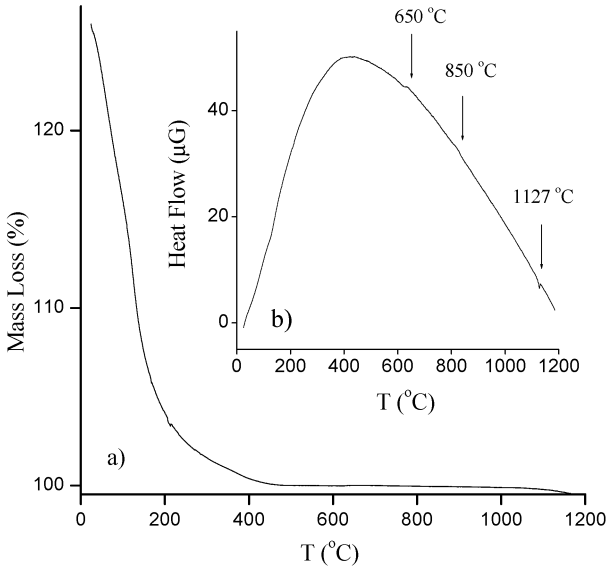

Figure 2. (a) TG data and (b) DTA data for the 0.13 M ZrW_2O_8 aerogel. Note that the lack of background subtraction in the DTA data results in a bell-shaped baseline.

0.13 M aerogel was selected for more thorough studies because it exhibits the largest initial surface area. Thermal treatments of the 0.13 M ZrW_2O_8 aerogel indicate that the high surface-to-volume ratio afforded by supercritical drying as well as the intimate mixing of constituents as part of the sol−gel process affect the product and allow kinetic control of the final phase. Short reaction times were used in an attempt to maintain the surface area of the starting aerogel.

When the aerogel is heated for 30 s, it remains amorphous at and below 700 °C. From 750 to 850 °C, trigonal ZrW_2O_8 forms and for temperatures 900 °C and above, the cubic phase forms. It should be noted that an identical heat treatment (900 °C, 30 s) of a xerogel (an ambiently dried gel which leads to a smaller surface area material) prepared from the very same sol does not result in the cubic phase at these low temperatures (∼900 °C). This important contrast shows the effect of morphology on phase formation.

The reaction at 900 °C is very sensitive to temperature and time. When the aerogel is heated in a larger batch, or in a covered crucible, there is a mixture of products. Heating for much longer than 30 s at 900 °C results in a mixture of phases, and much shorter times, or the use of an alumina crucible, does not allow for complete reaction. It is assumed that the entire sample is not able to reach 900 °C when an alumina crucible is used, or the reaction time is less than 30 s. For the materials with these incomplete, or partially complete reactions, part of the product is cubic, while the rest is amorphous; no intermediate phase was observed. It is believed that the sample reaches 900 °C in 30 s because the Pt crucible and small sample size allow for fast thermal equilibrium, while half-hour heat treatments at 850 °C do not form the cubic phase. Unfortunately, it was not possible to directly measure the actual temperature of the sample with time.

Reactions at 1000 and 1050 °C for 30 s lead to some decomposition of the cubic phase to the thermodynamically stable binary oxides, the higher annealing temperature having slightly larger phase fractions of the

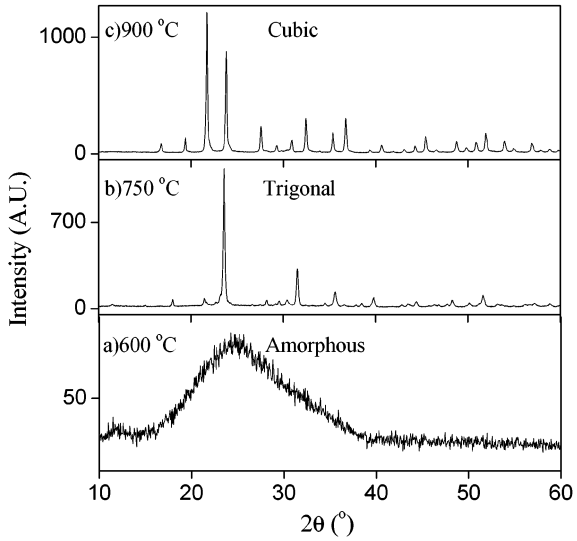

Figure 3. X-ray diffraction patterns of heat-treated ZrW_2O_8 aerogel.

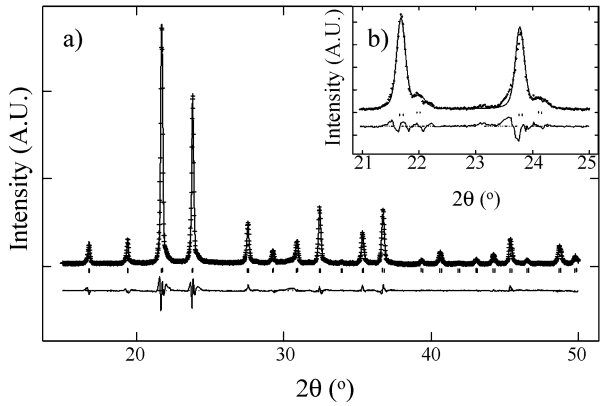

Figure 4. (a) Rietveld refinement of a particular sample of ZrW_2O_8 aerogel heated to 900 °C for 30 s. (b) LeBail intensity extraction of 0.13M3 (900 °C, 30 s) shows the hydrated cubic phases (upper tick marks). For both diffraction patterns, the crosses (+) are experimental points, the solid line represents the calculated pattern, the bottom line is the difference, and reflections are marked by (|).

noncubic phases. Heating the aerogel for as little as 5 min at 900 °C results in the binary oxides as the only phases present. On the other hand, at 700 °C, the trigonal phase is formed after 2.5 min, persists after a half-hour at that temperature, but has decomposed to the binary oxides within 12 h. As expected, the thermodynamic product, a mixture of ZrO_2 and $2WO_3$, is seen for extended heat treatments at all temperatures below 1100 °C.

Diffraction patterns (Figure 3) show the three different phases for the three different temperature regimes: (a) 600 °C (amorphous), (b) 750 °C (trigonal), and (c) 900 °C (cubic). For a particular 900 °C heat treatment, the results of Rietveld refinement agree well with the literature (Figure 4a).[13] For some preparations, a small amount (<5%) of the binary oxides (ZrO_2 + $2WO_3$) is seen in the X-ray diffraction patterns. Upon exposure to the atmosphere, the sample partially hydrates, as evidenced by a second phase (~20 molar %,

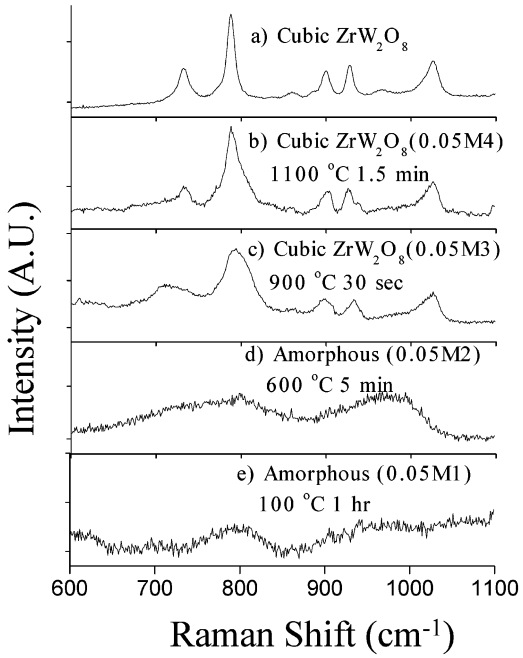

Figure 5. Raman spectra for various heat treatments (b, 1100 °C; c, 900 °C; d, 600 °C; e, 100 °C) of the 0.13 M ZrW_2O_8 aerogel. Highly crystalline cubic ZrW_2O_8 prepared from the xerogel (a) is shown for comparison.

$a = 9.031$ Å, Figure 4b) with a smaller lattice parameter. $ZrW_2O_8 \cdot xH_2O$ ($0 < x < 1$), previously reported by Duan et al., does not form under ambient conditions.[14] It is prepared by heating ZrW_2O_8 and H_2O under pressure at 180 °C, exhibits a volume contraction of up to 10%, and has a positive thermal expansion from −278 to 273 °C of approximately $+2 \times 10^{-6}$ C^{-1}. The hydration over time of a portion of our sample is a surface effect and demonstrates that some of the sample has a high surface-to-volume ratio.

The product of the 750 °C heat treatment is the trigonal ZrW_2O_8 phase. The diffraction pattern is very similar to the one reported by Wilkinson et al.[15] Although most of the largest reflections can be accounted for by using a model isostructural with trigonal $ZrMo_2O_8$, there are a large number of reflections that are not assigned. Some of these reflections can be accounted for by including a ~10% phase fraction of the cubic phase, but even so, there are observed reflections that are not modeled. In comparison, all of the reflections can be indexed on an expanded trigonal $ZrMo_2O_8$ cell (a, b, ~1.5c; $a = 9.8101(1)$ Å, $b = 9.8101(1)$ Å, $c = 17.602(2)$ Å, $\alpha = 90°$, $\beta = 90°$, $\gamma = 120°$), which is not a surprising expansion in this layered structure. The product of the 600 °C treatment shows only a broad peak centered around 25° 2θ ($d = 3.56$ Å) and so is termed amorphous (0.13M2).

Raman. Raman spectra of the 0.13 M aerogel at various heat treatments are compared to that of the cubic ZrW_2O_8 prepared from the xerogel (1100 °C, 1 h) in Figure 5. The spectrum for the amorphous 600 °C treated sample (0.13M2) only has broad bands and is similar to the spectrum of cubic ZrW_2O_8 after it becomes

(13) Evans, J. S. O.; Mary, T. A.; Vogt, T.; Subramanian, M. A.; Sleight, A. W. *Chem. Mater.* **1996**, *8*, 2809−2823.

(14) Duan, N.; Kameswari, U.; Sleight, A. W. *J. Am. Chem. Soc.* **1999**, *121*, 10432−10433.

(15) Wilkinson, A. P.; Lind, C.; Pattanaik, S. *Chem. Mater.* **1998**, *11*, 101−108.

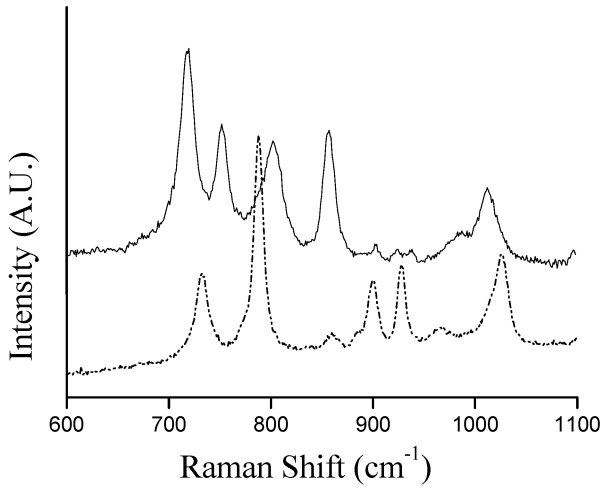

Figure 6. Raman spectra for the trigonal phase of ZrW_2O_8 (top, solid line) are shown along with the spectra for the cubic phase (bottom, dashed line) for comparison.

Table 2. Observed Raman Frequencies of the Trigonal and Cubic (from Ravindran et al.)[16] ZrW_2O_8 as Well as Frequencies for $ZrMo_2O_8$ (from Muthu et al.)[18]

cubic ZrW_2O_8 (cm^{-1})	trigonal $ZrMo_2O_8$ (cm^{-1})	trigonal ZrW_2O_8 (cm^{-1})	assignment
144	177	173	
234		214	lattice
		255	
271, 308	331	266	δ_{as}(Mo,WO_4)
331		397	
382	364	410	δ_s(Mo,WO_4)
733		719	
789	753	752	ν_{as}(Mo,WO_4)
859, 887	887	857	
901		902	
	948	923	
929	960	938	ν_s(Mo,WO_4)
966	1003	984	
1028		1012	

amorphous under pressure.[16] The 900 (0.13M3) and 1100 °C (0.13M4) treated samples have peaks previously reported to be due to the cubic phase that sharpen with temperature.[13,16,17] It should be noted that, for the amorphous samples, the strongest mode is at 145 cm^{-1} and can be assigned to lattice modes.

The Raman spectrum of the trigonal phase is reported for the first time here (Figure 6) and clearly shows a new phase distinct from the cubic phase. The observed Raman frequencies for the trigonal phase are compared to literature values for the cubic phase in Table 2. The assignments are made by comparison with other molybdates and tungstates, and as is customary, the modes are labeled in reference to the free WO_4 tetrahedra.[7,16,18] From higher to lower wavenumber, the Raman frequencies can be assigned to symmetric stretching, asymmetric stretching, symmetric bending, and asymmetric bending of the WO_4 tetrahedra. Below these, the frequencies are generally categorized as being due to lattice vibrations.

(16) Ravindran, T. R.; Arora, A. K.; Mary, T. A. *J. Phys.: Condens. Matter* **2001**, *13*, 11573−11588.
(17) Yamamura, Y.; Nakajima, N.; Tsuji, T.; Koyano, M.; Iwasa, Y.; Katayama, S. I. *Phys. Rev. B* **2002**, *66*, 014301.
(18) Muthu, D. V. S.; Chen, B.; Wrobel, J. M.; Anderson, A. M. K.; Carlson, S.; Kruger, M. B. *Phys. Rev. B* **2002**, *65*, 064101.

Table 3. Results from Fits to Absorption/Desorption Isotherms[a]

designation	temp (°C)	time (min)	Langmuir surface area (m^2/g)	equivalent surface area for SiO_2 (m^2/g)	average pore diameter (nm)
0.13M1	100	60	510(21)	4982	11
0.13M2	600	5	149(4)	1456	20
0.13M3	900	0.5	1.43(5)	15	48
0.13M4	1100	1.5	1.05(3)	10	14

[a] The average pore diameter was found using BJH analysis.

Table 4. Thermal Expansion Measurements of ZrW_2O_8 Materials

sample, run #	phase	temperature range °C	α ($\times 10^{-6}$ K^{-1})
0.05M2, 2	amorphous	50 to 150	−28.9
0.05M2, 2	amorphous	−50 to 50	9.2
0.05M2, 2	amorphous	−90 to 50	13.6
0.05M2, 2	amorphous	−150 to −90	48.8
0.05M3, 2	cubic	70 to 150	−1.4
0.05M3, 2	cubic	−50 to 50	−11.7
0.05M3, 2	cubic	−90 to 70	−8.8
0.05M3, 2	cubic	−150 to −90	18
0.05M4, 2	cubic	−50 to 50	−8.4
0.05M4, 2	cubic	−150 to 150	−6.1

Electron Microscopy. Electron microscopy was performed on two samples, the 600 °C (0.13M2) and the 900 °C (0.13M3) treated samples, to elucidate their morphology. The high-resolution TEM image of the aerogel 0.13M2 shows its airy spongelike morphology typical of an aerogel (Figure 7a). The higher magnification image (Figure 7c) of that particle confirms absorption/desorption results (Table 3) by depicting a pore with a diameter of about 20 nm and a wall thickness of 5−10 nm. Electron diffraction confirms the average amorphous structure (Figure 7b). The TEM study of 0.13M3, the aerogel heated to 900 °C for 30 s, indicates that the morphology has changed dramatically. Although there are regions that are still amorphous with a sponge like morphology, most of the sample is comprised of cubic ZrW_2O_8 crystallites that range from less than 50 nm to micrometers in diameter (Figure 8).

Thermal Expansion. The samples 0.13M2 (600 °C), 0.13M3 (900 °C), and 0.13 M4 (1100 °C) display different bulk thermal expansion with temperature. The measured coefficients of thermal expansion for these materials are summarized in Table 4. For the amorphous material with a high surface area, there are three temperature regimes (Figure 9a): (1) from −150 to −90 °C, (2) from −90 to 50 °C, and (3) from 50 to 150 °C. DSC results indicate no phase changes over this temperature range. The general shape and magnitude of the thermal expansion is repeatable and can be correlated with the amorphous structure and high surface area. A different high surface area amorphous aerogel prepared from the 0.35 M gel also demonstrated a similar variation of dimensions with temperature. The temperature region that shows negative thermal expansion occurs above room temperature and is 3 times greater than that of cubic ZrW_2O_8.

It should be reiterated that these data represent the measurement of bulk thermal expansion. Besides the possibility of a nanoscale effect inherent to the sample and due to the ∼5-nm-thick walls (e.g., the negative thermal expansion of gold nanoparticles[4]), the adsorbed

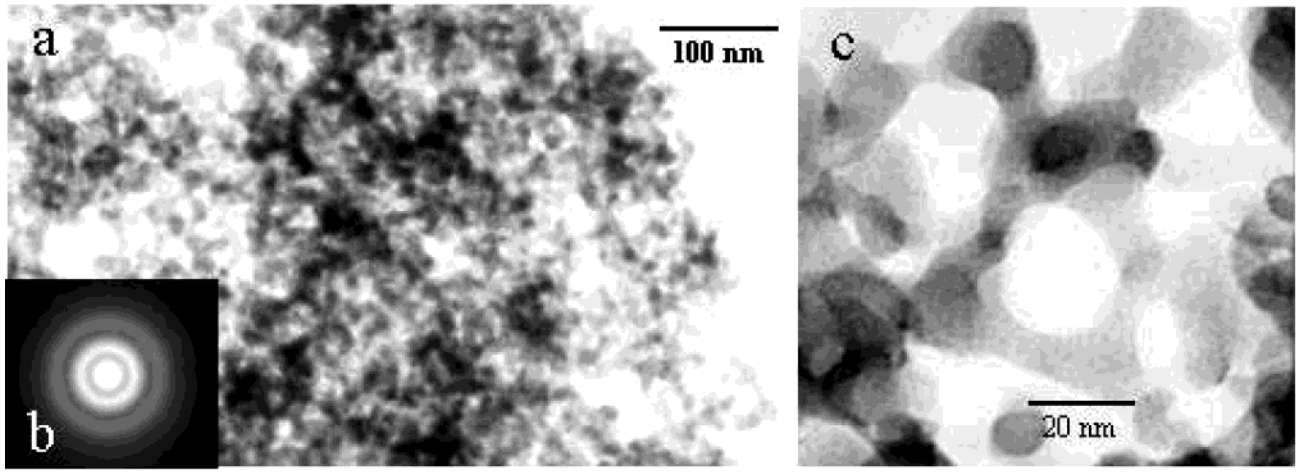

Figure 7. TEM images (a, c) of 0.13M2, the amorphous ZrW_2O_8 aerogel heated at 600 °C. (b) is the electron diffraction pattern of this sample.

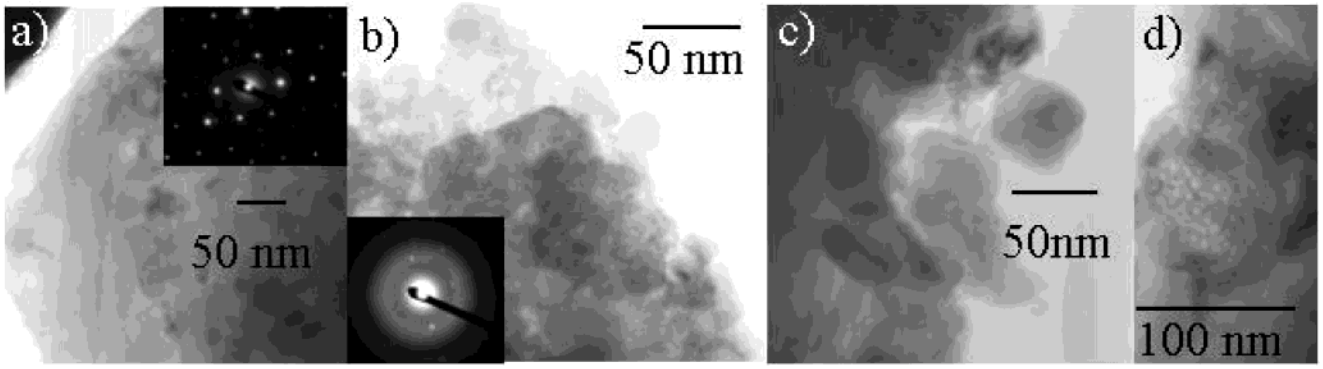

Figure 8. TEM images for 0.13M3 show particles ranging in size from (a) larger, (b) smaller, to (c) approximately 50 nm in diameter. (d) shows a porous region. Electron diffraction images confirm the cubic phase.

water inside the pores of the aerogel will have a large contribution to the thermal expansion. The thermal expansion of ice is 35×10^{-6} °C^{-1} at −100 °C[19] and, therefore, the existence of ice in the pores may explain the positive thermal expansion at low temperatures. The thermal expansion above 50 °C, where it changes sign and now has a large negative value, may also be due to water. If the framework were flexible, the loss of water molecules in the pores would cause an overall shrinkage of the structure. There are other possible explanations and contributions to the thermal expansion of this highly porous material. Theoretically, a material folding in on itself (into void regions, i.e., the pores) can result in negative thermal expansion.[20,21]

As shown in Figure 9b, there are also three temperature regimes for the cubic 900 °C heat-treated sample (0.13M3): 1) from −150 to −90 °C, (2) from −90 to 70 °C, and (3) from 70 to 150 °C. Like the amorphous sample described above, the thermal expansion coefficient below −90 °C is large and positive. The underlying reason for the low-temperature positive thermal expansion may be the same for both this cubic and the above-described amorphous ZrW_2O_8, that is, the presence of ice in the pores of the material. In the middle

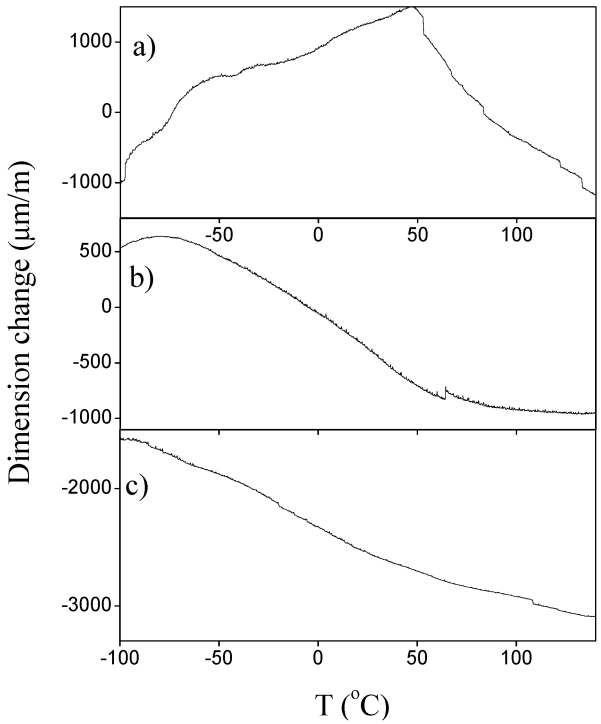

Figure 9. Dilatometer results for (a) 0.13M2 (600 °C, amorphous), (b) 0.13M3 (900 °C, cubic), and (c) 0.13M4 (1100 °C, cubic). Note that the discontinuities at ~50, 80, 120, and 130 °C (a), ~65 °C (b), and ~110 °C (c) are experimental artifacts and are not intrinsic to the sample.

(19) Rottger, K.; Endriee, A.; Ihringer, J. *Acta Crystallogr., Sect. B: Struct. Sci.* **1994**, *50*, 644−648.
(20) Gibiansky, L. V.; Torquato, S. *J. Mech. Phys. Solids* **1997**, *45*, 1223−1252.
(21) Sigmund, O.; Torquato, S. *J. Mech. Phys. Solids* **1997**, *45*, 1037−1067.

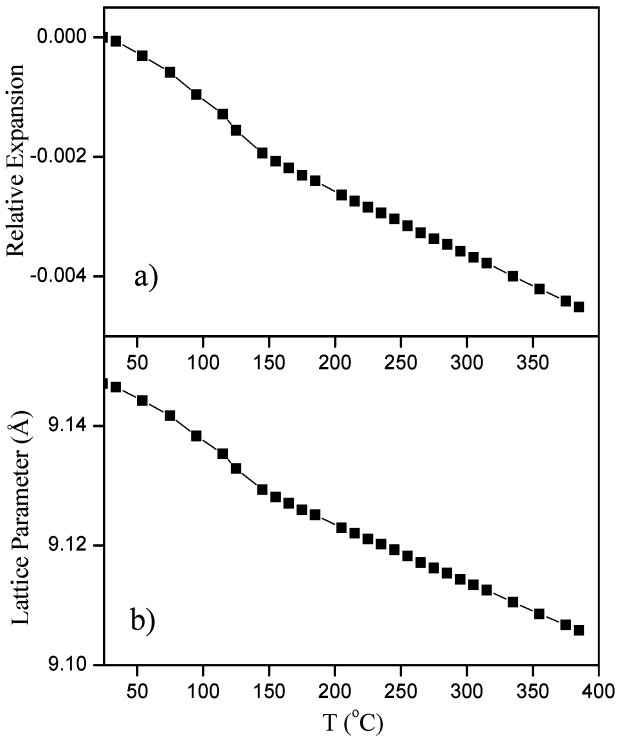

Figure 10. The (a) relative expansion [defined as $(l_{25} - l_T)/l_{25}$] and (b) lattice constant of the 900 °C heat-treated sample (0.13M3). The error in the lattice constant is smaller than the plotted points.

temperature range, the coefficient of thermal expansion has a large negative value as expected for cubic ZrW_2O_8. The change in slope above 50 °C could be due to the hydrated phase dehydrating. The cell parameter of cubic ZrW_2O_8 has been reported to contract linearly with increasing water content, and the fully hydrated polymorph ($ZrW_2O_8 \cdot H_2O$) displays a 10% volume decrease.[14] In our case, the increase in the unit cell upon dehydration from 9.008(1) to 9.1400(2) Å would contribute positively to the total thermal expansion.

The thermal expansion extracted from Rietveld refinement of variable temperature X-ray diffraction data on the cubic 900 °C heat-treated sample (0.13M3) agrees well with the literature. The large, almost linear decrease in lattice constant and relative expansion is well-documented (Figure 10). It is interesting to note that α [defined as $(l_{T2} - l_{T1})/(l_{T2}(T2 - T1))$ where l_{T1} is the lattice parameter at temperature 1, eq 1] decreases to a value of -16×10^{-6} °C^{-1} until the order−disorder phase transition (∼135 °C) when T1 = 25 °C (Figure 11a). Above the transition, α slowly approaches -12×10^{-6} °C^{-1}. When T1 is taken to be 175 °C, α has a constant value of -10.5×10^{-6} °C^{-1} above that temperature. These results from the refinement of variable temperature X-ray data do not coincide with the results from the dilatometric data presented above. The XRD data show no change in slope near 50 °C. Of course, X-ray diffraction just measures the ZrW_2O_8 crystalline phase and is not sensitive to contributions from impurity phases or amorphous material. It should be noted that the hydrated phase observed in the X-ray diffraction pattern at room temperature (Figure 4b) disappears upon heating.

In contrast to the dilatometric results of these two materials, the thermal expansion of the cubic ZrW_2O_8 (0.13M4, Figure 9c) is quite linear over the entire measured temperature range (−150 to 150 °C), and the measured coefficient of thermal expansion of -6.1×10^{-6} °C^{-1} agrees well with those reported previously in the literature ($\alpha = -13.5 \times 10^{-6}$ to -5×10^{-6} °C^{-1}).[22] This consistency with the literature values indicates that the dilatometer measurement gives expected results and that the expected bulk thermal expansion can be obtained from the exact same starting aerogel as was used for 0.13M2 and 0.13M3. At this time it is not clear whether the different bulk thermal expansion is a direct or indirect result of the morphology. What is clear from these measurements is that this synthetic route forms cubic ZrW_2O_8 that has the industrially useful bulk properties in less than 1.5 min.

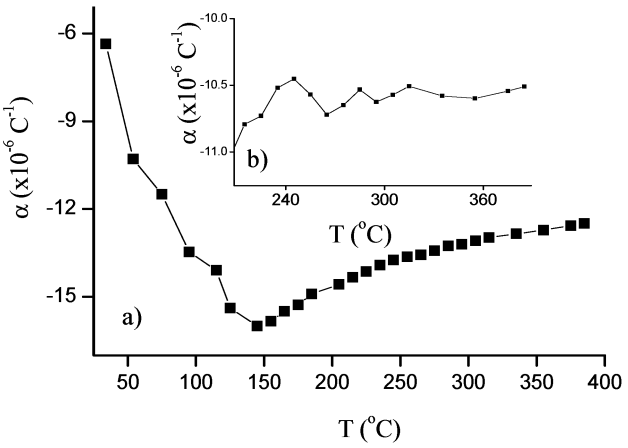

Figure 11. Thermal expansion coefficient (α) versus temperature when (a) T1 = 25 °C and (b) T1 = 175 °C for the 900 °C heat-treated sample (0.13M3). α is defined in the text (eq 1).

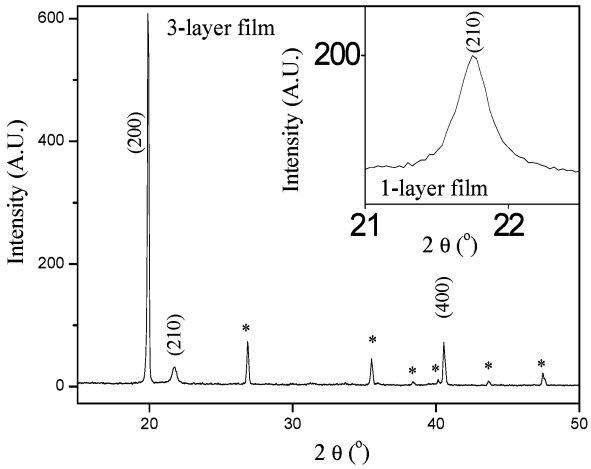

Figure 12. Diffraction pattern from a three-layer thin film. Reflections from ZrW_2O_8 are indexed and reflections from a $ZrSiO_4$-type phase are marked with a (*). The inset shows the only observed ZrW_2O_8 peak from a one-layer film.

Thin Films. Films prepared by spin coating a 0.5 M sol at 2000 RPM for 45 s were 0.25-μm thick. One-layer films were usually too thin to show diffraction peaks, although, occasionally, the 100% (calculated) reflection (210) of ZrW_2O_8 was observed (Figure 12, inset). For thicker multilayer films, diffraction lines of the cubic ZrW_2O_8 are clearly seen. The diffraction pattern of a three-layer film (0.75-μm thick, calcined at 1150 °C for

(22) Yilmaz, S. *Compos. Technol.* **2002**, *62*, 1835−1839.

0.5 h between layers) contains large (h00) (where $h = 2n$) reflections as well as a broader (210) reflection, indicating that the film is highly oriented. The unit cell edge ($a = 8.9$ Å) calculated from the (h00) reflections shows that the film was partially hydrated when the diffraction pattern was taken. This diffraction pattern (Figure 12) also shows diffraction peaks from a phase similar to $ZrSiO_4$ (JCDPS card 6-266), presumably due to an interfacial reaction between the film and substrate.

Conclusion

We have successfully prepared gels with the composition ZrW_2O_8. The gels were processed to form amorphous high surface area aerogels. From the aerogel, the cubic phase forms within 30 s at 900 °C and above. Below 900 °C the trigonal phase is formed. It is interesting that the cubic phase is the kinetic phase in this temperature range where it is thermodynamically unstable and that the aerogel morphology allows for its capture. This behavior shows that the precursor morphology affects phase formation. By taking advantage of the short reaction times and lower temperatures (900 °C, 30 s), we are the first to report the preparation of sub-micrometer cubic ZrW_2O_8 with negative thermal expansion properties. The ability to make small particle size ZrW_2O_8 is an important technological step in this field because mechanical milling of ZrW_2O_8 results in an amorphous material and the loss of the negative thermal expansion properties. The bulk thermal expansion properties are slightly different for the cubic phase formed at 900 °C than for the cubic phase formed at 1100 °C. This is most likely due to hydration effects that are observable due to the higher surface-to-volume ratio in the 900 °C sample. This difference can be minimized when forming composites by ensuring that the dehydrated polymorph is used.

Acknowledgment. We greatly appreciate the support of this research by Northrop Grumman Corporation and the National Science Foundation (DMR-0103952). We thank Prof. S. M. Haile and Dr. M. A. Thundathil for the use of the variable temperature diffractometer. We also thank Dr. J. Skelton and Prof. Zink for the collection of the Raman spectra.

CM034791Q